Fine-grained Lung Function Sensing based on Millimeter-Wave Radar

Shijie Han[1], Dongheng Zhang[1,2], Jinbo Chen[1], Haoyu Wang[1], Jinli Zhang[1], Qibin Sun[1], Yan Chen[1,2]
[1]School of Cyber Science and Technology, University of Science and Technology of China, Hefei, China
[2]Institute of Dataspace, Hefei Comprehensive National Science Center, Hefei, China
Email: {hsj1020, jinbochen, why1999, zhangjinli}@mail.ustc.edu.cn , {dongheng, qibinsun, eecyan}@ustc.edu.cn

***Abstract*—The COVID-19 pandemic has posed a significant threat to the health of elderly individuals, particularly those with respiratory conditions. Therefore, daily monitoring of lung capacity is necessary to assess the pulmonary condition and initiate timely treatment measures. This paper aims to explore an effective non-contact method for fine-grained pulmonary function sensing. Specifically, we propose to utilize millimeter-wave radar to contactless sensing of the overall chest and abdominal motion. Then the LUNet (Lung Unet) is constructed to recover the Expiratory Volume (EV) curves using the entire motion information of the chest and abdomen. Finally, the pulmonary function indicators are extracted based on the predicted EV curve directly. The experimental results demonstrate that the average correlation of the predicted EV curve is 96.74% and the mean relative errors for FEV1, FVC, and FEV1/FVC are 7.73%, 8.15%, and 6.70%, respectively. These results suggest that our method has the potential for clinical monitoring and assessment of respiratory diseases.**

***Index Terms*—millimeter wave radar, lung function, respiratory diseases, chest-abdominal movements, neural network**

I. Introduction

In 2021, FIRS released the third edition of the "Global Impact of Respiratory Disease" report, asthma and chronic obstructive pulmonary disease (COPD) are among the top five respiratory diseases worldwide [1]. These diseases are among the most common causes of illness, disability, and death globally. From 1990 to 2017, the global death toll from COPD increased by 23%. Currently, approximately 3 million people die from COPD each year [2]. The spread of smoking and the aging population, along with the declining mortality rates of other causes of death such as cardiovascular diseases, indicate that by 2060, there may be over 5.4 million deaths annually from COPD and related diseases [3]. The characteristic feature of these diseases is the presence of various types of airway obstruction. Spirometry is the most common pulmonary function test used to diagnose and monitor lung diseases, providing valuable information about lung health [4]. The current home spirometers are either too expensive ($>$\$2,000) or have low accuracy, potentially resulting in errors of $>$20% [5]. Furthermore, contact-based measurements increase the risk of cross-infection. With the prevalence of COVID-19, daily lung capacity measurements have become particularly important for timely diagnosis and treatment [6].

The development of more convenient, comfortable, and effective spirometer technology has always received significant attention in the medical community. While advancements have been made in contact-based methods [7, 8, 9] based on wearable technology, recent years have witnessed much interest in contactless lung function monitoring. Typically, contactless methods work by capturing chest wall single-point motion waveform and interpreting such information as indicators of pulmonary function. Acoustics technology is a viable solution for measuring lung function parameters [13, 14, 15, 16, 17]. But its usage requires an extremely quiet environment and is prone to interference from ambient noise. Recently, lung function monitoring based on wireless signals also emerged as a potential solution due to the contactless, privacy-preserving, comfortable user experience, as well as cost-effective deployability. [18] proposed extracting chest wall motion from the variations in WiFi signals and interpreting such information as indicators of pulmonary function.

However, relying solely on single-point motion data from the chest wall is insufficient to accurately describe the intrinsic characteristics of respiration. [19] implemented enhanced respiratory motion analysis by creating a 3D model of the whole chest and abdominal region. [20] demonstrated that the expansion of the upper and lower chest jointly correlated with all pulmonary function parameters. [21] found that the chest (upper and lower) and abdominal movements of most patients with chronic obstructive pulmonary disease (COPD) are reduced to varying degrees. [22] achieved promising results by estimating respiratory volume based on chest and abdominal movements together. [19], [20], [21], [22] indicate that there are different correlations between lung function and various regions within the entire chest and abdominal area. These works highlight the importance of analyzing the complete chest and abdominal motion in order to precisely extract intrinsic characteristics of breathing activity and enhance the accuracy of pulmonary function sensing.

Inspired by [25] that employs radio signals to comprehensively image torso surface motion, we extend a new dimension of wireless sensing by designing a contactless Fine-grained Lung Function system with millimeter-wave radar that exploits the relation between the overall chest and abdominal motion and lung functions. Specifically, the system depends on radar contactless sensing of the overall chest and abdominal motion, recovering the Expiratory Volume (EV) curves, and finally extracting the pulmonary function test indicators for lung

function evaluation. To do so, we first separate the reflections coming from different parts of the torso by beamforming. Then we project the space voxel signals into body surface motions imaging representation. To solve EV curves recovering problem, we propose a data-driven deep neural network that leverages the temporal-spatial features of body surface motions imaging input. Finally, corresponding pulmonary function indicators can be calculated based on the EV curves. We evaluate our system using a commodity radar sensor and conduct 150 experimental trials over 13 participants. The average correlation of the predicted EV curves is 96.74%. The mean relative errors for FEV1, FVC, and FEV/FVC are 7.73%, 8.15%, and 6.70%, respectively.

II. Materials and Indicators

A. Data Collection

We collect respiratory data from volunteers using the AWR1843 [26] millimeter-wave radar in synchronization with the GDX-SPR [27] respiratory device. Each of the 13 volunteers will perform 10-15 sessions of 30 seconds of breathing. Each session will include one deep breath, followed by normal breathing for the remaining time. The data collected during each session is divided into multiple segments of 512 frames, with 1-second equivalent to 100 frames. During the testing period, volunteers are required to sit with their backs against the chair back, maintaining an upright posture. They should hold the mouthpiece of the spirometer with their mouth and try to keep their upper body stable during the lung capacity test to minimize any interference from body movements on the overall chest and abdominal motion. Simultaneously, the millimeter-wave radar is positioned approximately 0.7 meters away from the volunteers and directed towards the chest and abdominal region.

B. Pulmonary Function Test (PFT) Indicators

Lung capacity measurement primarily generates the following three indicators for the clinical evaluation of pulmonary function:

- Forced Vital Capacity (FVC): FVC refers to the maximum amount of air that can be forcefully exhaled after taking a deep breath. It is an important measure of lung size and overall lung function.
- Forced Expiratory Volume in 1 second (FEV1): FEV1 represents the amount of air forcefully exhaled in the first second during an FVC test. It provides information about the rate at which air can be expelled from the lungs and is used to assess airflow limitation.
- FEV1/FVC ratio: This ratio is calculated by dividing the FEV1 value by the FVC value. It is used to assess the presence of airflow obstruction. A reduced FEV1/FVC ratio indicates the potential presence of a respiratory condition such as chronic obstructive pulmonary disease (COPD) or asthma.

In addition, this study introduces a new metric called the EV curve correlation, which is used to assess the similarity between the predicted EV curve and the original EV curve.

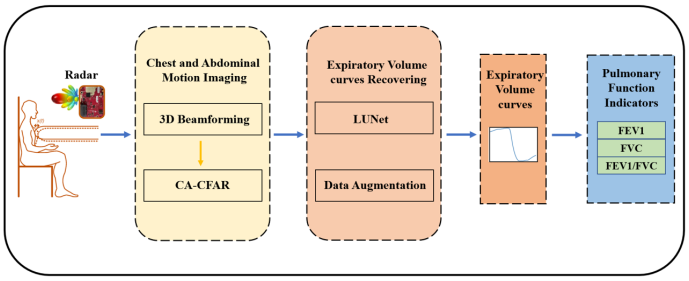

Fig. 1: System Overview.

Since the EV curve provides valuable information about respiratory characteristics, it enables a more comprehensive evaluation of lung function and enhances the accuracy of diagnosing respiratory conditions.

III. System Design

The system workflow is shown in the Fig. 1. It utilizes mm-wave radar to capture the signal variations of chest and abdominal movements during respiration. 3D beamforming and CA-CFAR techniques are employed to extract the chest and abdominal motion imaging. Then, by constructing LUNet (Lung Unet), the system recovers the accurate EV curves from the imaging inputs. Finally, corresponding pulmonary function indicators can be calculated based on the curves directly.

A. Chest and Abdominal Motion Imaging

3D Beamforming: By using an array of antennas in millimeter-wave radar and employing a frequency-modulated continuous wave (FMCW) system, we can map the propagation distance of the reflected signals to phase changes. Ultimately, through phase accumulation of the received signals in a virtual channel formed by different transmitting and receiving antennas, we can reconstruct the reflected signals from all positions in the entire space.

$$S(x,y,z,t) = \sum_{n=1}^{N}\sum_{t=1}^{T} y_{n,t} e^{j2\pi \frac{kr(x,y,z,n)}{c}} e^{j2\pi \frac{kr(x,y,z,n)}{\lambda}} \quad (1)$$

In the equation, N represents the number of virtual channels formed by different transmitting and receiving antennas. $y_{n,t}$ represents the received signal of virtual channel n at time t. k represents the frequency modulation slope, λ represents the wavelength of the RF signal, and $r(x,y,z,n)$ represents the round-trip propagation distance of the reflected signal from the three-dimensional spatial position (x,y,z) to the virtual channel n. Through the aforementioned computation of three-dimensional beamforming, the multi-channel time-domain signals are transformed into spatial domain representation. Therefore, the phase data of the signals in the chest and abdominal region contains respiratory information.

CA-CFAR: Since the human chest and abdomen are not standard cylindrical shapes, and to ensure stability during lung capacity testing, the subject needs to lean their back against the chair. As a result, the distances between different regions

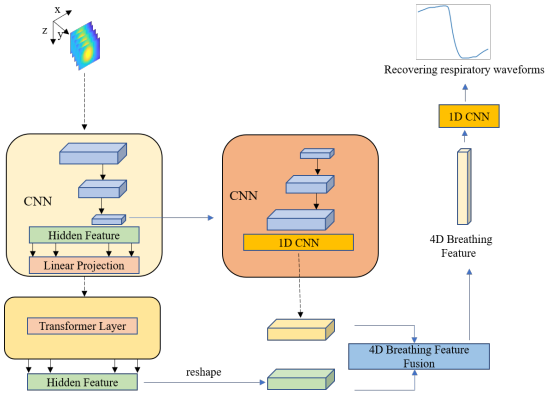

Fig. 2: LUNet architecture for Expiratory Volume curves recovering.

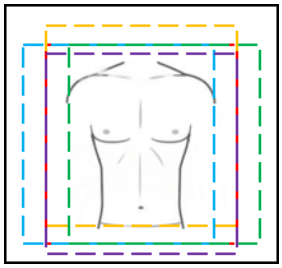

Fig. 3: Spatial data augmentation of the samples.

of the chest and abdomen and the millimeter-wave radar will vary. To accurately extract the motion plane of the chest and abdomen during breathing, given the X and Z coordinates, the signal amplitudes at different Y distances are summed, and the distance corresponding to the maximum signal intensity is considered as the region of the chest and abdomen. Additionally, to avoid interference from noise and clutter, the Cell Averaging-Constant False Alarm Rate (CA-CFAR) algorithm is employed to adaptively detect the target signals and finally form the chest and abdomen motion imaging.

B. Expiratory Volume curves Recovering

LUNet: The Unet network architecture can capture the contextual information of images and obtain multi-scale information, allowing it to accurately capture the respiratory features of different regions in the chest and abdomen. The Transformer network architecture is capable of capturing the dependencies between different positions in the input sequence, assigning weights to the influence of different regions in the chest and abdomen on lung function, the network structure is shown in the Fig. 2. By combining the Unet and Transformer network architectures, we can learn the nonlinear correlation between the overall region of the chest and abdomen and lung function.

Data Augmentation: Insufficient data during the training process of deep neural networks often leads to the problem of overfitting. Hence, it is essential to employ data augmentation techniques to enhance the robustness of the model. In this study, two data augmentation methods are utilized. The first

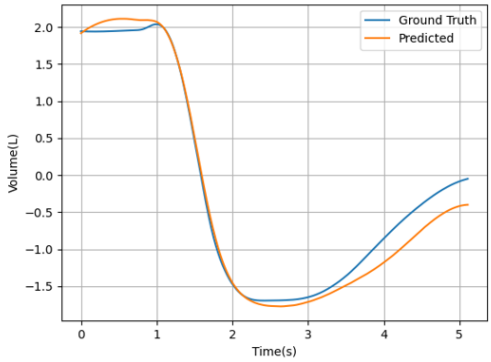

Fig. 4: Predicted Expiratory Volume curve and the original Expiratory Volume curve.

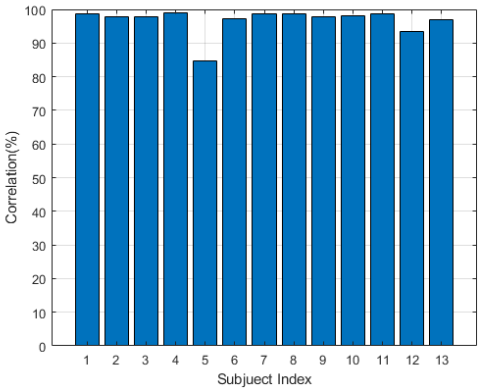

Fig. 5: The correlation between the predicted Expiratory Volume curve and the original Expiratory Volume curve.

method is temporal augmentation, which involves linearly expanding or compressing time to extend or shorten each respiratory cycle effectively. The second method is spatial augmentation, as illustrated in the Fig. 3, which introduces different spatial regions while ensuring coverage of the chest and abdominal areas. This is equivalent to introducing different noise interferences, which helps the model better learn and understand the intrinsic features of abdominal movements.

IV. Performance Evaluation

The leave-one-out cross-validation method is used to evaluate the performance of lung function detection during the training of the LUNet. This method involves selecting one individual's data as the test set and using the data from the remaining individuals as the training set. The process is repeated for each participant, and the average results are obtained at the end. This approach allows for a comprehensive evaluation of the network's performance by ensuring that each individual's data is used both for training and testing, thus providing a more robust assessment of the lung function detection performance.

A. Performance of the predicted Expiratory Volume curves

The results of the EV curves recovered by LUNet and the original EV curves are shown in Fig. 4, the two curves almost completely overlap. The correlation between the predicted EV curves and the original EV curves for different subjects is shown in Fig. 5. The average correlation can reach 96.74%, indicating a high similarity between the predicted and original EV curves. Therefore, the predicted EV curves can be used to extract relevant pulmonary function indicators and assist in the diagnosis of pulmonary diseases.

B. Performance of the estimated pulmonary function indicators.

We also evaluate the performance of pulmonary function indicators based on the predicted EV curve results. We compare our method with the SpiroFi in [18], which extracts single-point chest wall motion from radio signal variations and interprets this information as pulmonary function indicators using Bayesian regularized neural networks. As demonstrated in Fig. 6, our approach significantly improves system performance with respect to mean relative errors in FEV1, FVC, and FEV1/FVC. Specifically, we achieve mean relative errors of 7.73%±1.61%, 8.15%±1.69%, and 6.70%±2.61% for each indicator respectively. In comparison, the SpiroFi method yielded larger mean relative errors in FEV1, FVC, and FEV1/FVC at 14.90%±7.62%, 16.45%±10.41%, and 14.93%±8.03% respectively. These results clearly indicate that our method outperforms SpiroFi across all three pulmonary function indicators, demonstrating better robustness.

C. Ablation experiment

To demonstrate that using the phase of the entire chest and abdomen region as input yields better results than using the phase of a single point, an ablation experiment is conducted. In this experiment, the maximum signal intensity point is selected from the previously extracted chest and abdomen plane, and the phase information of that point is used as input to the LUNet. The performance comparison between single-point and whole-region is shown in the Fig. 7. The FEV1, FVC, and FVC/FEV1 obtained from single-point phase input are 16.92%, 9.83%, and 15.26%, respectively. On the other hand, the FEV1, FVC, and FVC/FEV1 obtained from whole-region phase input are 8.60%, 5.71%, and 6.68%, respectively. It can be observed that the whole-region phase input has significant advantages over the single-point phase input, indicating that learning respiratory features from the whole region of the chest and abdomen can significantly improve the performance of lung function detection.

To validate the crucial role of the transformer architecture in capturing the spatial relationships between the chest and abdomen regions, the transformer structure is removed from the network to observe if the network could accurately learn the features of EV curves. A comparison of performance is made between the LUNet without the transformer structure and the LUNet with the transformer structure, as shown in the Fig. 8. Without the transformer structure, the values of FEV1,

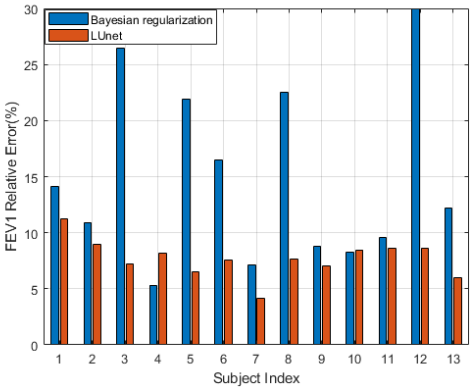

(a) FEV1

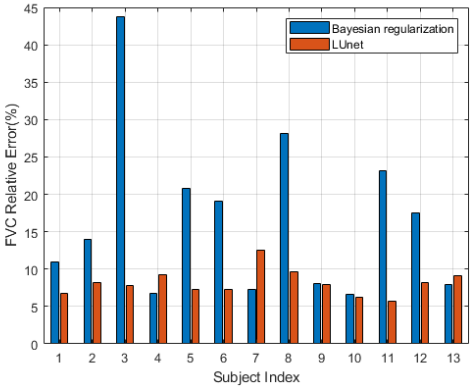

(b) FVC

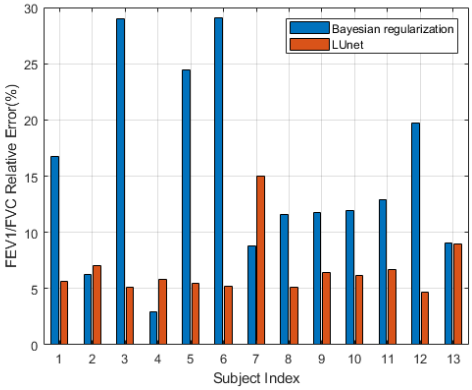

(c) FEV1/FVC

Fig. 6: Comparison of Spirofi [18] and our method for estimating pulmonary function indicators.

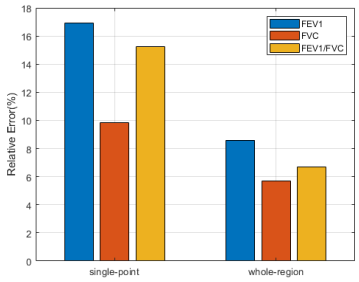

Fig. 7: Performance comparison between single-point and the whole-region.

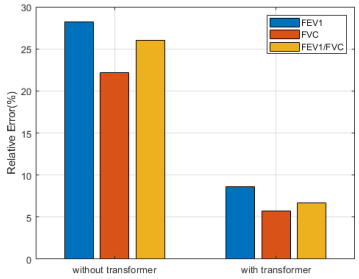

Fig. 8: Performance comparison between without and with the transformer structure

FVC, and FVC/FEV1 are 28.24%, 22.19%, and 26.02%, respectively. With the transformer structure, the values of FEV1, FVC, and FVC/FEV1 are 8.60%, 5.71%, and 6.68%, respectively. It is evident that the transformer structure effectively establishes spatial relationships among various points in the chest and abdomen, enabling the accurate learning of respiratory characteristics.

V. Conclusion

This study investigated the fine-grained perception of lung function using mmWave radar. By studying the whole-region of the chest and abdomen and utilizing the LUNet, the intrinsic respiratory features were learned, resulting in highly restored EV curves and low errors in pulmonary function indicators. The mean relative errors for FEV1, FVC, and FEV1/FVC were 7.73%, 8.15%, and 6.70%, respectively. Comparatively, the error of pulmonary function indicators in clinics is typically around 5%, indicating that the proposed method has the potential to become a reliable solution for daily monitoring.

Acknowledgments

This work was supported by National Key R&D Programmes under Grant 2022YFC0869800 and 2022YFC2503405, National Natural Science Foundation of China under Grant 62201542 and 62172381, fellowship of China Postdoctoral Science Foundation under grant 2022M723069, and the Fundamental Research Funds for the Central Universities.

References

[1] *Forum of International Respiratory Societies.* http://firsnet.org
[2] Li X, Cao X, Guo M, et al. Trends and risk factors of mortality and disability adjusted life years for chronic respiratory diseases from 1990 to 2017: systematic analysis for the Global Burden of Disease Study 2017[J]. bmj, 2020, 368.
[3] Global Initiative for Chronic Obstructive Lung Disease (GOLD). Global strategy for the diagnosis, management, and prevention of chronic obstructive pulmonary disease: 2022 report [internet publication].
[4] Miller M R, Hankinson J, Brusasco V, et al. Standardisation of spirometry[J]. European respiratory journal, 2005, 26(2): 319-338.
[5] Hegewald M J, Gallo H M, Wilson E L. Accuracy and quality of spirometry in primary care offices[J]. Annals of the American Thoracic Society, 2016, 13(12): 2119-2124.
[6] Milanese M, Corsico A G, Bellofiore S, et al. Suggestions for lung function testing in the context of COVID-19[J]. Respiratory medicine, 2021, 177: 106292.
[7] Gupta S, Chang P, Anyigbo N, et al. mobileSpiro: accurate mobile spirometry for self-management of asthma[C]//Proceedings of the First ACM Workshop on Mobile Systems, Applications, and Services for Healthcare. 2011: 1-6.
[8] Chu M, Nguyen T, Pandey V, et al. Respiration rate and volume measurements using wearable strain sensors[J]. NPJ digital medicine, 2019, 2(1): 8.
[9] Carspecken C W, Arteta C, Clifford G D. TeleSpiro: A low-cost mobile spirometer for resource-limited settings[C]//2013 IEEE Point-of-Care Healthcare Technologies (PHT). IEEE, 2013: 144-147.
[10] Lewis G F, Gatto R G, Porges S W. A novel method for extracting respiration rate and relative tidal volume from infrared thermography[J]. Psychophysiology, 2011, 48(7): 877-887.
[11] Yu M C, Liou J L, Kuo S W, et al. Noncontact respiratory measurement of volume change using depth camera[C]//2012 Annual International Conference of the IEEE Engineering in Medicine and Biology Society. IEEE, 2012: 2371-2374.
[12] Reyes B A, Reljin N, Kong Y, et al. Tidal volume and instantaneous respiration rate estimation using a volumetric surrogate signal acquired via a smartphone camera[J]. IEEE journal of biomedical and health informatics, 2016, 21(3): 764-777.
[13] Goel M, Saba E, Stiber M, et al. Spirocall: Measuring lung function over a phone call[C]//Proceedings of the 2016 CHI conference on human factors in computing systems. 2016: 5675-5685.
[14] Larson E C, Goel M, Boriello G, et al. SpiroSmart: using a microphone to measure lung function on a mobile phone[C]//Proceedings of the 2012 ACM Conference on ubiquitous computing. 2012: 280-289.
[15] Wang A, Sunshine J E, Gollakota S. Contactless infant monitoring using white noise[C]//The 25th Annual International Conference on Mobile Computing and Networking. 2019: 1-16.
[16] Nandakumar R, Gollakota S, Watson N. Contactless sleep apnea detection on smartphones[C]//Proceedings of the 13th annual international conference on mobile systems, applications, and services. 2015: 45-57.
[17] Nandakumar R, Gollakota S, Sunshine J E. Opioid overdose detection using smartphones[J]. Science translational medicine, 2019, 11(474): eaau8914.
[18] Yu G, Wang M, Zhao P, et al. SpiroFi: Contactless Pulmonary Function Monitoring using WiFi Signal[C]//2022 IEEE/ACM 30th International Symposium on Quality of Service (IWQoS). IEEE, 2022: 1-10.
[19] Aliverti A, Lacca D, LoMauro A. Quantitative Analysis by 3D Graphics of Thoraco-Abdominal Surface Shape and Breathing Motion[J]. Frontiers in Bioengineering and Biotechnology, 2022, 10: 910499.
[20] Reddy R S, Alahmari K A, Silvian P S, et al. Reliability of chest wall mobility and its correlation with lung functions in healthy nonsmokers, healthy smokers, and patients with COPD[J]. Canadian respiratory journal, 2019, 2019.
[21] Kaneko H, Shiranita S, Horie J, et al. Reduced chest and abdominal wall mobility and their relationship to lung function, respiratory muscle strength, and exercise tolerance in subjects with COPD[J]. Respiratory care, 2016, 61(11): 1472-1480.
[22] Raoufy M R, Hajizadeh S, Gharibzadeh S, et al. Nonlinear model for estimating respiratory volume based on thoracoabdominal breathing movements[J]. Respirology, 2013, 18(1): 108-116.
[23] *MmWave Radar Applications and Advantages.* https://resources.system-analysis.cadence.com/blog/msa2022-mmwave-radar-applications-and-advantages

[24] *Lung function tests.* https://app.pulsenotes.com/medicine/respiratory/notes/lung-function-tests
[25] Chen J, Zhang D, Zhang D, et al. MMCamera: an imaging modality for future RF-based physiological sensing[C]//Proceedings of the 28th Annual International Conference on Mobile Computing And Networking. 2022: 894-896.
[26] *AWR1843.* https://www.ti.com.cn/product/cn/AWR1843
[27] *Go Direct Spirometer User Manual.* https://www.vernier.com/manuals/gdx-spr/